Mechanism of OmpG pH-dependent gating from loop ensemble and single channel studies

Alan Perez-Rathke[1,*], Monifa A. Fahie[2,3,*], Christina Chisholm[2,3], Jie Liang[1,§], and Min Chen[2,3,§]

[1] Department of Bioengineering, University of Illinois at Chicago, Chicago, Illinois 60607, USA
[2] Department of Chemistry and [3] Molecular and Cellular Biology Program, University of Massachusetts Amherst, Amherst, Massachusetts 01003, USA
* Both contributed to the work equally
[§] To whom correspondence should be addressed
Email: mchen1@chem.umass.edu, jliang@uic.edu

ABSTRACT

Outer membrane protein G (OmpG) from *Escherichia coli* has exhibited pH-dependent gating that can be employed by bacteria to alter the permeability of their outer membranes in response to environmental changes. We developed a computational model, Protein Topology of Zoetic Loops (Pretzel), to investigate the roles of OmpG extracellular loops implicated in gating. The key interactions predicted by our model were verified by single-channel recording data. Our results indicate that the gating equilibrium is primarily controlled by an electrostatic interaction network formed between the gating loop and charged residues on the lumen. The results shed light on the mechanism of OmpG gating and will provide a fundamental basis for the engineering of OmpG as a nanopore sensor. Our computational Pretzel model could be applied to other outer membrane proteins that contain intricate dynamic loops that are functionally important.

INTRODUCTION

The outer membrane proteins of gram-negative bacteria control the permeability of the membrane barrier, which is required for bacterial survival.[1] With only one exception,[2] all outer membrane proteins have β-barrel structures. Many of these outer membrane proteins possessing a pore-like barrel are classified as porins, through which solute molecules can diffuse across the outer membrane along a concentration gradient.[3] Porins are essential for nutrient uptake and are also effective barriers against potentially harmful chemicals.[4] Changes in the permeability of outer membrane proteins have been found in some antibiotic-resistant pathogenic bacteria.[5,6]

Outer membrane protein G (OmpG) is a nonspecific porin that allows small molecules to diffuse across the membrane.[7,8] The expression of OmpG is constitutively suppressed in *Escherichia coli,* but it can occur in some mutant strains.[9,10] OmpG expression is present at low levels in *Salmonella, Shigella*, and *Pseudomonas* species.[9] Electrophysiological characterization of OmpG shows that at neutral pH it is a mostly open pore that fluctuates spontaneously between the open and closed conformations.[7] This gating behavior is sensitive to pH, as decreasing the pH below 6 shifts the pore to a more closed state.[7] The conformational change triggered by low pH was later directly observed in atomic force microscopy studies of OmpG on native *E. coli* lipid membrane.[11] The pH-dependent gating of OmpG represents an excellent model for how bacteria can control the permeability of their outer membrane in response to environmental changes.

Structural studies have provided great insight into the key element that mediates this spontaneous and pH-dependent gating.[12] OmpG is a barrel-shaped protein composed of 14 β-strands that forms a relatively large channel on the membrane.[8,12,13] The diameter of the barrel is 14 Å at its widest, on the periplasmic side, and gradually decreases to 8 Å on the extracellular side.[14] OmpG contains seven short turns on this periplasmic side and seven long loops at its extracellular side. Two crystal structure conformations of OmpG have been obtained at pH 5.6 and pH 7.5.[12] These studies revealed that at pH 5.6, loop 6 is collapsed into the lumen,

representing a closed conformation, while at pH 7.5, loop 6 projects away from the lumen, representing an open conformation. However, because the protein contacts in the crystal structure are made through the loop regions, it is not clear whether different loop conformations could be selected from the lattice packing during the crystallization process. Nuclear magnetic resonance studies of OmpG have shown a much shorter barrel and longer, more disordered extracellular loops that could also invade into the lumen.[13,15] To test if the conformation of loop 6 is the dominant contributor to the gating, a quiet OmpG mutant (qOmpG) was created in which loop 6 was tethered to a neighboring strand to prevent it from bending into the lumen.[14] At pH 8.5, the gating activity of qOmpG was reduced by 95% compared to the wild-type protein. To reduce the flexibility of loop 6 using a different approach, loop 6 was pinned to the membrane via a lipid anchor, which also decreased the gating frequency at pH 6.0 by more than 95%.[16] Together, these findings indicate that loop 6 is the major gating loop whose conformational changes result in current fluctuations in the electrical recording measurements.

Although previous studies have identified loop 6 as the predominant player in OmpG gating, the molecular mechanism controlling loop 6, and how pH modulates the gating equilibrium, remain unclear. Yildiz et al. postulated that residues His231 and His261 (Fig.1a) are the pH-sensor elements.[12,17] They suggested that protonation of the two histidines at acidic pH generates a repulsive force that destabilizes β-strand 12, causing it to partially unfold. The unfolded β-strand 12 can then join loop 6 to form an elongated loop to cover up the entrance of the lumen. Although the mechanism of repulsion between two histidines appears plausible for pH-dependent gating, it cannot explain the fact that gating signals are also observed at neutral and high pH, where repulsion would not occur. In addition, NMR studies indicate that other loops may affect the dynamics of loop 6,[15] although it is unclear how loop-loop interactions may modulate the movement of loop 6 in a pH-dependent manner.

Unraveling the OmpG gating mechanism has additional significance beyond improving our understanding of how bacteria modulate the outer membrane permeability. As OmpG possesses a unique monomeric structure, it has become attractive as a nanopore sensor compared to other classic trimeric porins OmpF and OmpC.[14,18-20] Our recent works have demonstrated the use of OmpG gating behavior for highly specific protein homologue sensing.[19,21,22] Thus, understanding of OmpG gating may also guide the design of OmpG-based nanopore sensors for new applications.

In the present work, we have developed a computational model, Pretzel (Protein Topology of Zoetic Loops), to identify structural determinants that control OmpG gating behavior. Our results show there are two highly charged patches inside the barrel region serving as regulators of OmpG gating. Our results indicate the electrostatic interaction network formed between loop 6 and the charged residues on the lumen can either attract or repel loop 6 from the pore entrance. The roles of residues in these two discrete regions were verified in mutants by single channel recording. The gating equilibrium is controlled by the strength of the two opposing forces, which can be modulated by pH through protonation and deprotonation of the critical aspartate, glutamate and histidine residues in the OmpG lumen and on loop 6.

MATERIALS AND METHODS

Cloning of OmpG mutants. Single or multiple mutations were introduced into OmpG by mutagenesis polymerase chain reaction (PCR) using the plasmid pT7-OmpGwt as the template.[19] All primers (Eurofins MWG Operon) for each mutagenesis PCR are listed in Supplemental Information Table S1. Paired forward and reverse primers were used in a 1:1 molar ratio. The PCR reaction mixtures were subjected to DpnI digestion for 3 hours at 37°C to degrade the parental plasmid. Chemically competent *E. coli* DH5α cells were then transformed with the PCR mixture, and colonies containing the desired mutant constructs were miniprepped and confirmed by DNA sequencing.

Expression and purification of OmpG proteins. All OmpG proteins were prepared using a previously described protocol.[19,23] Briefly, cells transformed with the desired construct were grown in 250 mL of LB medium at 37°C until the OD_{600} reached 0.6. Thereafter, the culture was induced by adding isopropyl β-D-1-thiogalactopyranoside to a final concentration of 0.5mM. After 3 hours, the cells were harvested for protein purification or frozen at −20°C for future use. To purify the OmpG proteins, cells were resuspended in 50mM Tris-HCl (pH 8.0), 1.0mM EDTA and lysed via sonication. The lysate was centrifuged at 20,000*g* for 20 min. The resulting pellet was resuspended in 30 mL 50mM Tris-HCl (pH 8.0), 1.5M urea buffer and incubated at 22°C for 10 min. Afterwards the mixture was centrifuged at 20,000*g* for 20 min, and the inclusion body was solubilized in 50mM Tris-HCl (pH 8.0), 8M urea by stirring for 30 min. The mixture was centrifuged at 20,000*g* for 20 min. The supernatant was loaded to a Q sepharose (GE Healthcare) anion exchange column equilibrated in 50mM Tris-HCl (pH 8.0), 8M urea. All OmpG proteins were eluted in 50mM Tris-HCl (pH 8.0), 200mM NaCl, 8M urea. Purified OmpG was then diluted with refolding buffer containing 50mM Tris-HCl (pH 9.0), 3.25% (w/v) octyl glucoside (GoldBio) in a 2:3 protein-to-buffer (v/v) ratio. Samples were then incubated at 37°C for 3 days. The refolding efficiency was determined by heat denatured mobility shift on SDS-polyacrylamide gel electrophoresis.

To prepare refolded qOmpG, a previous protocol was followed.[14] The qOmpG construct was purified under reducing conditions in 8M urea, 5mM dithiothreitol buffer. qOmpG was then diluted in 5mM dithiothreitol refolding buffer and incubated at 37°C for 3 days. The dithiothreitol was removed from the refolded sample using a desalting column equilibrated with 50mM Tris-HCl (pH 8.0), 0.01% (w/v%)n-dodecyl-D-maltoside. Cu(*o*-phenanthroline)$_2$ was prepared by mixing $CuSO_4$ and *o*-phenanthroline in a 1:4 (mol:mol) ratio and then mixed with the protein solution at a final concentration of 2mM. The mixture was incubated with gentle rotation for 15 min at 23°C. Ethylenediaminetetraacetic (EDTA) was added at a final concentration of 10mM to quench the copper-catalyzed oxidation reaction. The sample was then exchanged to 50mM Tris-HCl (pH 8.0),

2% octyl glucoside buffer using a centricon with a 10 kDa molecular weight cut-off to remove excess EDTA, copper, and *o*-phenanthroline. The qOmpG sample was used immediately or stored in 20% glycerol at −80°C.

Single-channel recording of OmpG proteins. Single-channel recording of OmpG was performed as previously reported.[19] Briefly, experiments were performed using a black lipid membrane. Hexadecane dissolved in pentane (10%, v/v) was added to the aperture and the pentane allowed to evaporate. Buffer solution was added to each chamber, and then 1,2-diphytanoyl-sn-glycerol-3-phosphocholine (Avanti Polar Lipids) was dropped onto the surface to form a monolayer in each chamber. A buffer of 1M KCl and 20mM sodium acetate, 20mM sodium phosphate, or 20mM Tris-HCl was used to maintain a pH of 5, 6, or 7, respectively. A Ag/AgCl electrode was immersed into each chamber with the *cis* chamber grounded. The solution in each chamber was pipetted below and above the aperture slowly to promote lipid bilayer formation on the aperture. OmpG proteins were added into the *cis* chambers. A voltage higher than 200 mV was applied until a single OmpG pore inserted into the bilayer. The voltage was then lowered to 50 mV for recording. The signals were filtered with a Bessel filter at 2 kHz and then acquired at a sampling rate of 100 μs after digitization with a Digidata 1320A/D board (Axon Instruments).

Single-channel gating analysis. OmpG gating properties were analyzed in Clampfit 10.7 (Molecular Devices) using the single-channel search from a 20 s section of a trace (unless otherwise stated). The extracted dwell times of the open and closed state were used to calculate the open probability, the average interevent duration ($\boldsymbol{\tau}_{open}$), and the average event duration ($\boldsymbol{\tau}_{closed}$). The open probability is the total time in the open state divided by the total time analyzed. The average interevent duration ($\boldsymbol{\tau}_{open}$) was extracted from at least 300 interevent time. The interevent times were plotted in a histogram and fit with a single exponential function to calculate the average. The event duration ($\boldsymbol{\tau}_{closed}$) was similarly calculated.

To generate the two-dimensional event density map, a 10 s trace was analyzed using the single channel search command to collect the gating events by using Clampfit. The events were distributed on a two-dimensional density contour map based on their dwell time and amplitude by using Origin Pro.

Computational modeling of the conformational states of OmpG loops. OmpG has extracellular loops of nontrivial lengths (12 and 18 residues for loops 1 and 6, respectively), and it is difficult to accurately sample a large and diverse structural ensemble of loops.[16,24] Recent developments in loop sampling techniques such as distance-guided sequential chain-growth Monte Carlo and multi-loop Distance-Guided Chain-Growth Monte Carlo (mDiSGro) now make it possible to examine in detail the equilibrium ensemble of loop structures.[24,25,40] To understand the role of OmpG loops, we first extensively sampled 10^5 conformations of OmpG loops 1, 2, 3, 5, 6, and 7 using the mDiSGro loop-modeling algorithm with modifications (see Supplemental Information, Methods). Loop 4 was excluded as it already has a well-formed helical secondary structure in both template structures (2iwv and 2iww). In addition, all residues in the barrel region were fixed so that large-scale sampling of the loops could be achieved. The presence of the excluded volume of the membrane bilayer was imposed through steric clash detection against membrane atoms placed using CHARMM-GUI (see Supplemental Information, Methods).[26] Through introduction of a distance-based bias, the mDiSGro algorithm can significantly improve sampling efficiency.[24,25] Overall, we were able to generate about 600,000 and 300,000 multi-loop samples from both template PDB structures 2iwv and 2iww[12,27]

Next, we corrected sampling bias introduced in mDiSGro by separately clustering and resampling the 2iwv and 2iww loop ensembles. First, we reduced the dimensionality of each loop ensemble using principal component analysis to 95% variance retention; this was necessary to improve computational efficiency. We then separately clustered each loop ensemble in the PCA space using a streaming affinity propagation algorithm with Euclidean distance metric.[28,29] This

resulted in 547 and 467 clusters for the 2iwv and 2iww loop ensembles, respectively. We then uniformly resampled from the 547 clusters of the 2iwv loop ensemble to generate a set of 75,000 multiloop conformations, with roughly equal representation from each cluster (see Supplemental Information, Methods). We repeated the resampling procedure on the 467 clusters of the 2iww loop ensemble to generate an additional 75,000 samples. We combined both resampled ensembles into a unified ensemble for subsequent modeling of OmpG pH gating. In short, we constructed a combined loop ensemble consisting of 150,000 OmpG sample conformations with equal representation of both 2iwv and 2iww barrels. After clustering and resampling, the resulting ensemble approximates a uniform distribution over the full space of geometrically realizable OmpG loops. We assume that this carefully constructed and balanced loop set can adequately capture the spatial configurations of OmpG loops relevant for gating.

To model the effects of varying pH conditions, we first calculated the acid dissociation constants of all ionizable residues in each of the 150,000 OmpG sample loop conformations using the PROPKA3 method.[30] We then used NAMD[31] to protonate each ionizable residue if the computed pK_a was greater than the specified pH condition. Next, we used NAMD's conjugate gradient minimizer to relax all hydrogens as well as loop side chains in generalized Born implicit solvent for 66 steps using the CHARMM36 force field[32] with a 16 Å cutoff radius. We then calculated the total energy of each OmpG sample with only loop atoms unfixed. We performed the protonation, relaxation, and energy computation procedure for both pH 5 and pH 7. We retained the 5,000 lowest-energy OmpG samples at each pH level for further analysis.

We examined the gating states of each of the 5,000 lowest-energy OmpG sample conformations through topological analysis using the CASTp method.[33] We used a probe radius of 2.75 Å to simulate passage of a K^+ ion.[34] If we observed a membrane-spanning tunnel with mouth openings both above and below the lipid bilayer, we designated the OmpG sample as an "open" (conducting) conformation, otherwise we designated the sample as a "closed" (non-conducting) conformation.

We note the X-ray crystal structure PDBs 2iwv and 2iww are also consistent with our energy model. Specifically, the 2iwv “open” conformation captured at approximately pH 7 has the lowest energy when compared to our simulated pH 7 ensemble, and the 2iww “closed” conformation captured at approximately pH 5 has the lowest energy when compared to the simulated pH 5 ensemble. While the crystal structures are used as templates for all generated conformations and are not directly included in our gating analysis, they are overall consistent with our findings.

All computational modeling source code is available via our git repository at https://bitbucket.org/aperezrathke/ompg-public. In addition, we developed SCOBY, an efficient C++ clustering toolkit, which is freely available at https://bitbucket.org/aperezrathke/scoby.

RESULTS

Gating behavior of OmpG proteins.

To investigate whether loop 6 indeed dictates pH gating, we studied how a previously characterized quiet OmpG mutant (qOmpG) responded to acidic conditions. qOmpG contains a disulfide bond and a D215 deletion.[14] The disulfide bond tethers loop 6 to the neighboring strand 13, thus preventing loop 6 from bending into the lumen. The single-channel recording results were consistent with previous research[14] showing that, at pH 7, the qOmpG protein exhibits significantly decreased gating activity compared to OmpG. More importantly, the pH-dependent gating was absent in qOmpG: its open probability at pH 5 remained 99%, the same as it was at pH 7. These data supports that the motion of loop 6 is responsible for conducting the pH-dependent gating.

We then tested the two-histidine repulsion hypothesis that has been suggested to control gating.[12] We generated two mutants containing single mutation H231A and H261A, as well as a mutant containing double mutation H231A/261A which refolded well (Fig. S2). We investigated the gating behavior of these proteins using single-channel recording. For simplicity, only traces recorded at −50 mV are shown and discussed here. The open probability of the two single mutants

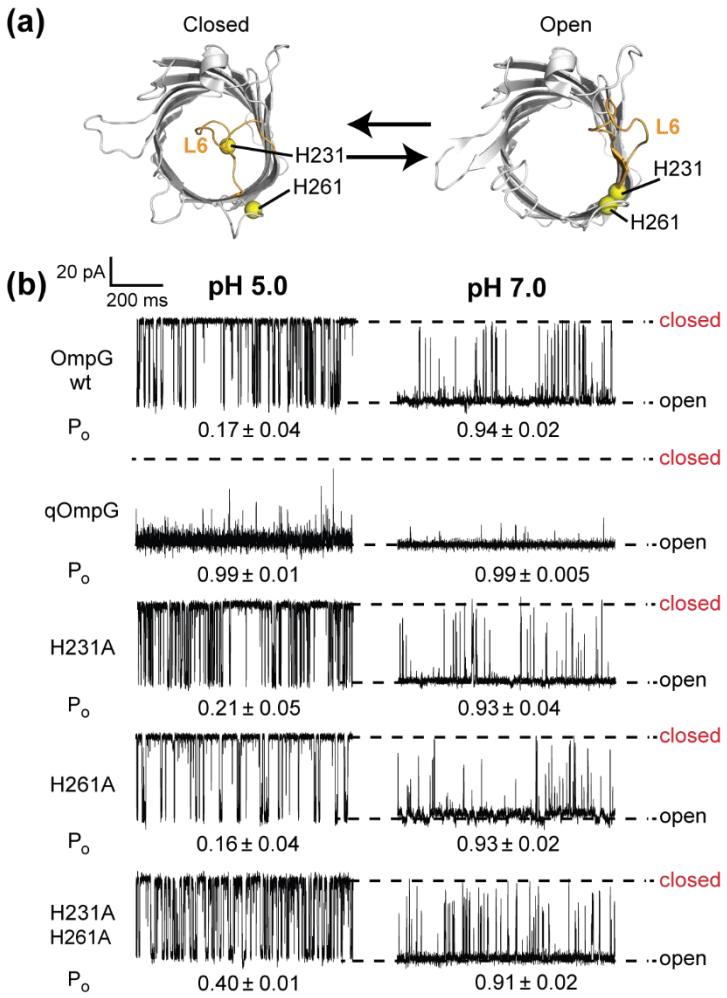

Figure 1. Gating behavior of OmpG variants at pH 5 and pH 7. (a) Structure of OmpG in the open (2iwv) and closed (2iwv) states. Residues H231 and H261 are highlighted as yellow balls. (b) Electrophysiology traces of OmpG proteins. The open probabilities (P_o) are shown under the respective traces. Data were acquired at −50 mV in 1.0M KCl buffer containing 20mM sodium acetate for pH 5 or 20mM Tris-HCl for pH 7. OmpG proteins were recorded with a 2 kHz Bessel filter at a sampling rate of 100 µs. The average P_o was calculated from at least five independent traces and the error indicates the standard deviation.

H231A and H261A was similar to that of OmpGwt at pH 7. It was expected that the gating of all three histidine mutants would not respond to the pH change due to the loss of the repulsive force between the two histidines. Surprisingly, the open probability of H261A decreased to 0.16 ± 0.04 at pH 5, almost indistinguishable to the 0.17 ± 0.04 of OmpGwt. In comparison, the open probability of H231A was reduced to 0.21 ± 0.05, slightly higher than that of H261A. At pH 5, the double mutation (H231A/H261A) OmpG had a more than 2-fold increase in open probability

compared to OmpGwt. These data points out that while residues H231 and H261 may contribute to the pH-sensitivity in OmpG, it is unlikely that they do so via a mechanism of repulsion between two protonated histidine residues,[12] because if that were the case then mutating either H231 or H261 would disrupt the repulsion and result in a pH-insensitive OmpG protein. Instead, we observed that both H231A and H261A responded strongly to pH change. We therefore surmise that repulsion is not the dominant factor that triggers pH gating, and that residues H231 and H261 may contribute to the pH gating via interacting with other residues nearby.

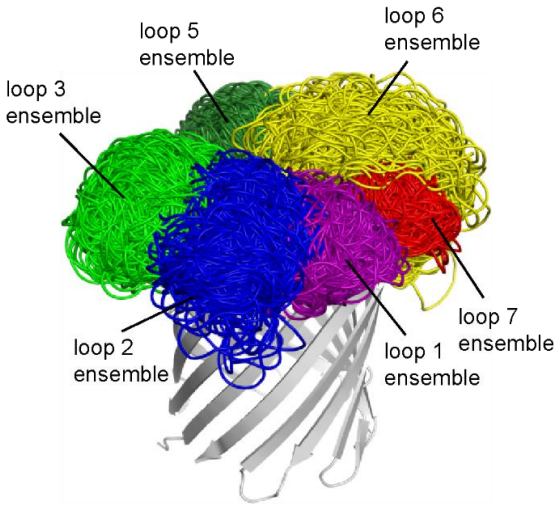

Figure 2. Extracellular view of the 547 representative OmpG conformations among the ~600,000 conformations generated using the 2iwv barrel structure. These exemplar representatives were obtained using the streaming affinity propagation method of clustering[29]. After performing the same clustering procedure on the ~300,000 conformations generated using the 2iww barrel, an additional 467 representative OmpG conformations (not pictured) were obtained.

Computationally generated ensemble of loop structures reveal geometric basis of pH-gating.

We then use a modified mDiSGro loop-modeling algorithm to sample the conformations of OmpG loops. To reiterate, we generated approximately 600,000 conformations using barrel template 2iwv and 300,000 conformations using barrel template 2iww. We corrected sampling bias by separately clustering the 2iwv ensemble and the 2iww ensemble, followed by uniformly resampling from the cluster sets; this resulted in a balanced ensemble of 150,000 conformations

used for physical modeling and analysis. Fig 2 illustrates the 547 representative OmpG conformations obtained through clustering the 2iwv ensemble.

To determine the geometric basis of gating activity, we investigated the conformational ensembles of OmpG loops at both pH 5 and pH 7. Of the 5,000 lowest-energy OmpG conformations captured at pH 7, approximately 74% are in the open state; i.e., there exists a passageway for K^+ ion conductance. In contrast, only about 45% of the 5,000 lowest-energy conformations are in the open state at pH 5. These findings are consistent with the overall pattern of decreasing open probability with decreasing pH that was empirically observed in this study and elsewhere.[7,15]

We further developed a simple image processing technique to infer which loops were spatially occluding the OmpG lumen among the low-energy closed conformations (Fig. S1). Our analysis showed that at pH 5, loop 6 was occluding the lumen in ~94% of the low-energy closed ensemble. Additionally, loop 1 was occluding in 5% of the ensemble. At pH 7, loop 6 was occluding the lumen in 78% of the low-energy closed ensemble; loop 1 and loop 2 were primarily occluding among the remaining 17% and 4% of the ensemble, respectively.

Electrostatic interactions between loop 6 and the positive patch region stabilizes the closed gating state.

To gain broad mechanistic understanding of OmpG gating, we examined electrostatic loop-to-loop and loop-to-barrel interactions that consistently favored the closed state. Specifically, we examined electrostatic interactions that were stabilizing towards the closed state at 95% confidence levels (Supplemental Information, Methods).[35] We identified interactions between loop 6 and particular sets of residues in the OmpG barrel that consistently favored the closed state at pH 5 and pH 7 (Fig. 3a,c). Specifically, loop 6–to-barrel interactions exhibited the most prominent stabilizing effects towards the closed state among all loop-to-barrel and loop-to-loop interactions,

although intra-loop electrostatic interactions in loop 6 also consistently favored the closed state at pH 5 and pH 7.

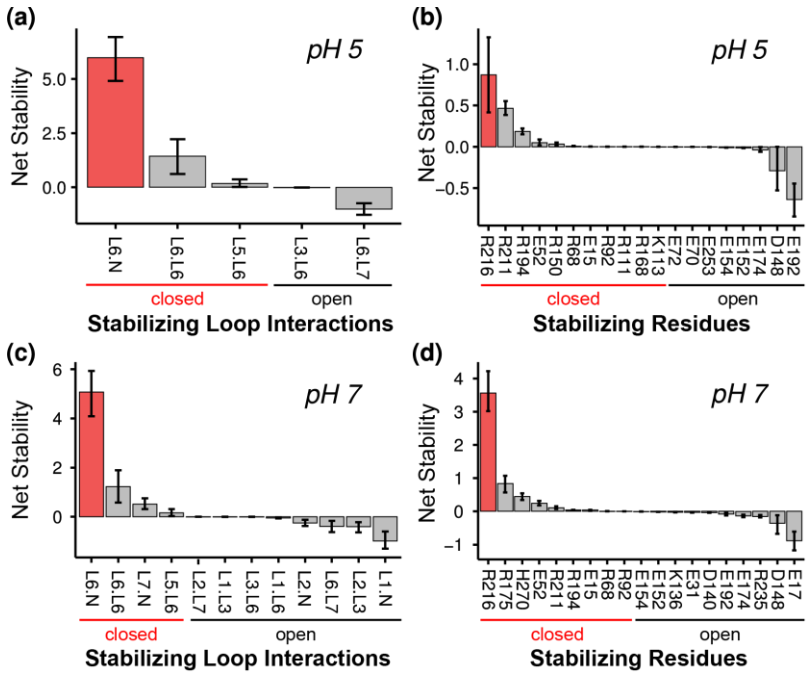

Figure 3. Computed net stabilities for OmpG loops and residues. The net stability is defined as the difference in median electrostatic energies between open and closed sample conformations (see Supplemental Information, Methods). (a,c) Loop-to-loop (L.L) and loop-to-barrel (L.N) interactions providing significant net stabilities at (a) pH 5 and (c) pH 7. The label 'N' in 'L.N' represents the non-loop barrel region. The most significant stabilizing interaction L6.N is colored in red. (b,d) Non-loop barrel residues with significant stability contributions at (b) pH 5 and (d) pH 7. The most significant residue contributing to L6.N stability at both pH 5 and 7 is colored in red.

We identified specific loop-interacting residues along the OmpG barrel that consistently favored the closed state (Supplemental Information, Methods). At pH 5, residues R211 and R216 exhibited the strongest interactions favoring the closed state among all barrel residues (Fig.3b,d). Additional significant residues favoring the closed state at pH 5, however with lower stability values, are R194, R150, R68, R92, R111, R168 and K113. The positive residue R216 also exhibited strong stabilizing effects towards the closed state at pH 7 (Fig. 3d). Interestingly, at both pH 5 and pH 7, the residues identified as stabilizing the closed state included positively charged

arginines (9 out of 13) and one lysine (Fig. 3b,d). Thus, we hypothesized that these multiple positive residues may work cooperatively to stabilize the closed state.

Probing the role of the positively charged patch by single-channel recording.

The computational analysis has pointed out a group of positively charged residues that strongly stabilize the closed state through interaction with loop 6. These positively charged residues appear to form a positive patch consisting of two clusters of arginines and lysines at the lumen (Fig. 4a). Cluster I, consisting of R68, R92, R111, K113 and R150, is located at the lumen opposite to loop 6, while cluster II, consisting of R194, R211 and R216, is located on the same side as loop 6. Because of the close proximity of R68 and R235 to cluster I and cluster II, we also include these two residues in our investigation.

To probe the role of the positive patch in OmpG gating, we mutated all nine residues from both positive clusters R68-R236 and each individual cluster R68-R150 and R194-R235 separately. However, none of these mutant proteins refolded well (Fig. S3). Thus, we mutated only two residues at a time from each cluster, and found that double mutants R111S/K113S and R211S/R216S exhibited satisfactory refolding efficiency. After considering these findings, we created the quadruple mutant R111S/K113S/R211S/R216S, which also refolded well (Fig. S3). All these positive-cluster mutants had an increased open probability at all pH levels compared to OmpGwt (Fig. 4b,c). OmpG with mutations on the opposite side of loop 6, R111S/K113S, showed higher open probability than the mutant R211S/R216S. The mutant containing residues from both positive clusters had an additive effect, as the mutant R111S/K113S/R211S/R216S exhibited the highest open probabilities: 2.65-, 1.27-, and 1.03-fold higher than those of OmpGwt at pH 5, 6, and 7, respectively (Fig. 4c).

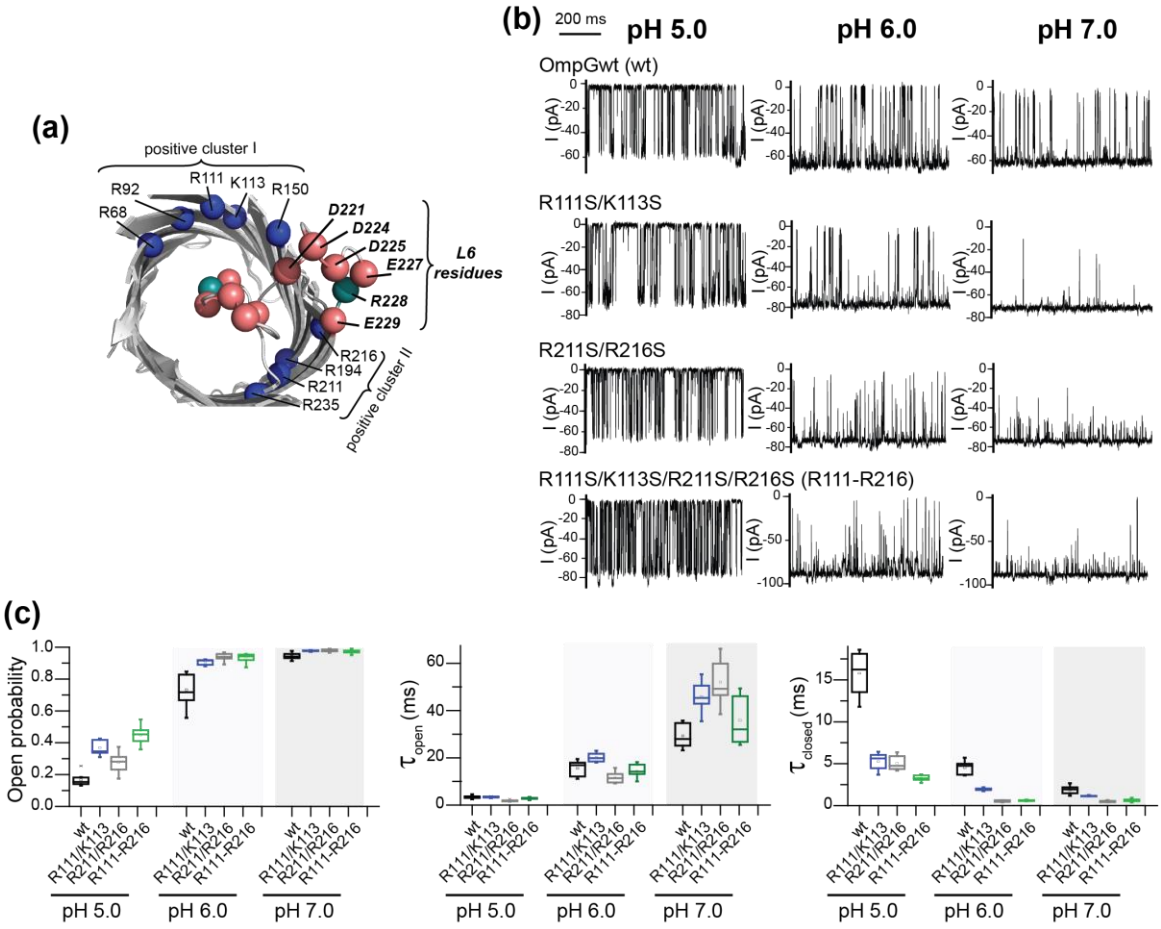

Figure 4. Role of the positive patch in OmpG gating. (a) Structure of OmpG. Loop 6 of the open (2iwv) and closed (2iww) conformations are overlaid on the OmpG barrel from the open structure. The Cα of the residues of the positive patch are highlighted as blue balls. The Cα of the negatively charged residues on loop 6 are depicted as pink balls, and the positively charged residue, as a teal ball. (b) Single-channel current recording of wild-type and mutant OmpG pores at different pH levels. Data were acquired at −50 mV in 1.0M KCl buffer containing 20mM sodium acetate for pH 5, 20mM sodium phosphate for pH 6, or 20mM Tris-HCl for pH 7. (c) Comparison of the open probability, interevent duration (τ_{open}), and event duration (τ_{closed}) of OmpG pores. The box and whisker plots were constructed from at least five independent measurements.

The open probability of the OmpG constructs describes a global effect on the gating equilibrium. However, it does not reveal specific details on the stability of the open or closed conformations that are affected by the mutations. Therefore, we analyzed the average dwell time of the open (τ_{open}) and closed (τ_{closed}) states of OmpG proteins (Fig. 4c) (Fig. S4&S5, Table S2). Compared to the wild type, the positive patch mutations showed no significant effect on τ_{open} at pH 5 or 6, but they increased the τ_{open} value at pH 7. However, the τ_{closed} of all three mutants was

significantly reduced at all pH conditions. Particularly at pH 5, the quadruple mutant showed a 5-fold decrease in τ_{closed}. These experiments, combined with our computational analysis, suggest that the positive patch is important for stabilizing the closed state at all pH conditions through electrostatic attraction with loop 6. At neutral pH, these positive residues may be also implicated in destabilizing the open state. Note that although the quadruple mutant only shifted the gating equilibrium to the open state 2-fold at pH 5, there were still five positive residues remaining at the lumen in this mutant, which may compensate for the role of the mutated residues. Thus, we expect that the positive patch contributes to stabilizing the closed state to a much greater extent than the mutants have revealed. In summary, our results strongly suggest that the electrostatic attractions between the negative residues of loop 6 and the positive patch are responsible for stabilizing the closed conformation of OmpG.

Negative residues exhibit significant change in protonation state at low pH.

While we have identified the residues responsible for stabilizing the closed state with high confidence, we found that the loop-barrel interactions favoring the open state are weak and more distributed; most barrel residues do not have a strong stabilizing effect towards the open state (Fig. 3b,d). Furthermore, non-patch residue E192 exhibited the strongest interactions favoring the open state among all barrel residues at pH 5, but this effect was only weakly significant at pH 7.

The positive patch mutants displayed strong pH-dependent gating similar to that of OmpGwt, which suggests that residues in the positive patch are not the pH-sensing element. This result is not surprising, as the guanidinium group of arginine has been reported to have an unusual ability to maintain the fully protonated state under all physiological conditions, such that its neutral state has not been unambiguously observed.[36] To identify the residues that can sense pH change, we examined residues that have significantly different protonation states when the pH is lowered from 7 to 5. Specifically, we constructed 95% confidence intervals for the difference in proportion

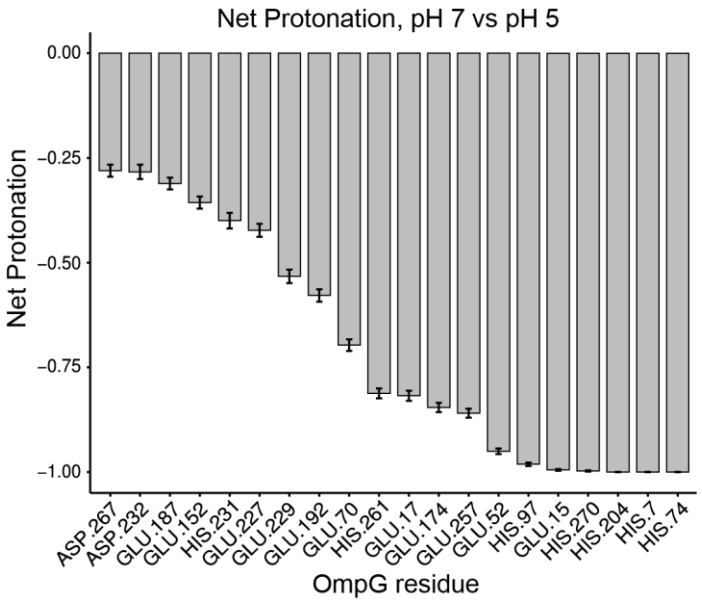

Figure 5. Computational net protonation for OmpG residues. Net protonation is defined as the difference in proportion of protonated states among low-energy samples at pH 7 and the proportion of protonated states among low-energy samples at pH 5. Whiskers were computed using adjusted bootstrap 95% confidence intervals (see Supplemental Information, Methods). Only the top 20 most significant residues are shown (see Fig. S6 for all significant residues). Negative values indicate that the residue is more frequently protonated at pH 5 relative to pH 7. For example, a value of −1 indicates the residue was 100% protonated at pH 5 and 0% protonated at pH 7 in our simulations.

of protonated states among low-energy conformations at pH 7 compared to the proportion of protonated states among low energy conformations at pH 5 for each ionizable residue. Confidence intervals that did not cross the 0-axis after multiple test corrections were deemed significant (Supplemental Information, Methods). As expected, several histidine residues, H7, H74, H97, H204, and H270, were the most likely to gain a proton, as well as H261 and, to a lesser degree, H231 (Fig. 5). Thus, we generated two mutants H270Y and H97S and tested these mutants in single-channel recording (Fig. S7). Our data indicated that neither H270 nor H97 significantly affected OmpG pH-gating: both mutants had behavior similar to that of OmpGwt (Fig. S7). Interestingly, several glutamate residues (E17, E174, E257, E52, E15) were also highly likely to gain protons and become uncharged. Analysis of the OmpG structure revealed that glutamate residues E15, E17 and E52 are spatially co-located, along with residue E31, forming a dense

patch of negative charge in the barrel opposite to loop 6 (Fig. 6a). Thus, we hypothesized that the protonation state of the negative patch may strongly affect the OmpG gating.

Probing the role of the negatively charged patch in pH-dependent OmpG gating by single-channel recording.

To explore the role that the negatively charged patch plays in OmpG gating, we exchanged all four glutamate residues to the neutral amino acid serine (Fig. 6a). The mutant E15S/E17S/E31S/E52S (E15S-E52S) exhibited drastically increased gating activity at all pH conditions (Fig. 6b). Strikingly, the open probability of the E15S-E52S mutant at pH 7 was 0.30 ± 0.03, which is close to the open probability of OmpGwt at pH 5, which is 0.17 ± 0.04 (Fig. 6c). Analysis of the average dwell times of the open and closed states of the E15S-E52S mutant reveals that the mutations altered both states: they decreased the τ_{open} by 3.6-, 6.7- and 8.3-fold and increased the τ_{closed} by 1.1, 2.3, and 4.8-fold at pH 5, 6, and 7, respectively. This result indicates that the negative patch is responsible for stabilizing the open state and destabilizing the closed state. Given that loop 6 has five net negative charges, our results suggest that the negative patch may alter the gating equilibrium towards the open state by repelling loop 6 from the pore entrance.

The effect of the mutations diminishes noticeably at pH 5. The τ_{closed} of the mutant is indistinguishable from that of OmpGwt, and the τ_{open} of the mutant is 3.6-fold lower than that of OmpGwt at pH 5 compared to the 8.3-fold at pH 7. This result suggests that in OmpGwt the repulsion between the negative patch and loop 6 is significantly weakened under acidic pH conditions, such that its behavior is similar to that of the OmpG E15S-E52S mutant. This result is consistent with our computational model, in which the negative patch was found to be protonated at pH 5, thus reducing its repulsion of loop 6. Taken together, our results strongly indicate that the negative patch is a key pH-sensing component of OmpG.

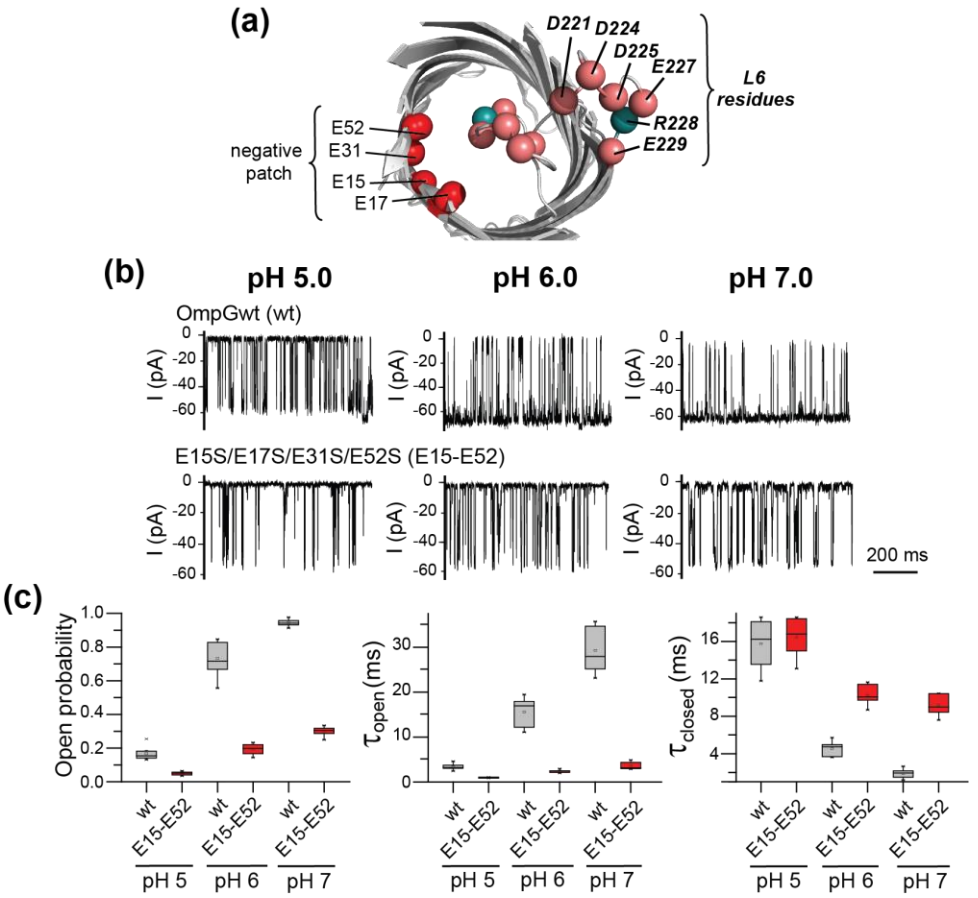

Figure 6. Role of the negative patch in OmpG gating. (a) Structure of OmpG. Loop 6 of the open and closed conformation are overlayed on the OmpG barrel. The Cα of the residues of the negative patch are highlighted as red balls. The Cα of the negatively charged residues on loop 6 are depicted as pink balls, and the positively charged residues, as teal balls. (b) Single-channel current recording of OmpG pores at different pH levels. Data were acquired at −50 mV in 1.0M KCl buffer containing 20mM sodium acetate for pH 5, 20mM sodium phosphate for pH 6, or 20 mM Tris-HCl for pH 7. (c) Comparison of the open probability, interevent duration (τ_{open}), and event duration (τ_{closed}) of OmpG pores. The box and whisker plots were constructed from at least five independent measurements.

Charged patches modulate the gating conformations.

The current traces of OmpG proteins revealed that the mutations not only affected the dwell times of the open and closed states, but also strongly altered the current amplitudes of the gating events (Fig. S8). The gating events of the wild type OmpG; the mutant R111S-R216S, in which the positive patch is disturbed; and the mutant E15S-E52S, in which the negative patch is disturbed; are displayed in a two-dimensional histogram showing the current blockage and the dwell time (Fig. 7). For wild type OmpG, the events varied from 50% to 100% blockage, with the majority at 100% blockage at pH 5 and 6 (Fig. 7b). While at pH 7 the event distribution slightly

decreased to 40% to 90%, with the majority at 90% blockage. For the positive patch mutant R111S-R216S, the amplitude of the events was mainly at 100%, as it was for OmpGwt. The gating events of this mutant have decreased amplitudes at pH levels above 6 compared to OmpGwt. At pH 6.0, the amplitudes of the events varied from 20% to 90%, with a dominant population close to 40%. At pH 7, the majority of the gating events only blocked the current by less than 30%. In contrast, the majority of the gating events for E15S-E52S showed 100% blockage for all pH conditions (Fig.7).

Although the amplitude of the gating events did not precisely correlate with the conformational substates of OmpG, it is reasonable to assume that the events of higher amplitude arose from narrower constriction sites formed by the bending of loop 6 towards the lumen. Importantly, the amplitude of the events correlated closely with dwell time. The dwell times for events with less than 90% blockage are shorter than the dwell times for events with 100% blockage. This suggests that the fully closed states represented by the 100% blockage events are more stable than the partially closed states represented by the lower amplitude (<90%) events. This may be because, in the fully closed states, loop 6 bends over the pore and forms multiple interactions with the R68-R150 cluster located on the opposite side of the lumen, as well as the nearby R211-R235 cluster. In the partially closed states, loop 6 may be only slightly tilted towards the pore entrance as a result of attraction to the positive R211-R235 cluster.

At pH 7, the R111S-R216S mutant only showed lower amplitude (<30%) events. This suggests that loop 6 was unable to collapse into the lumen due to the very weak interactions between loop 6 and the remaining residues of the positive patch. In contrast, loop 6 in the E15S-E52S mutant could form strong interactions with the lumen and fully obstruct the pore, even at pH 7. These results indicate that when the repulsion between loop 6 and the negative patch is strong at high pH 7, loop 6 in the mutant R111S-R216S is unable to adopt the closed conformation

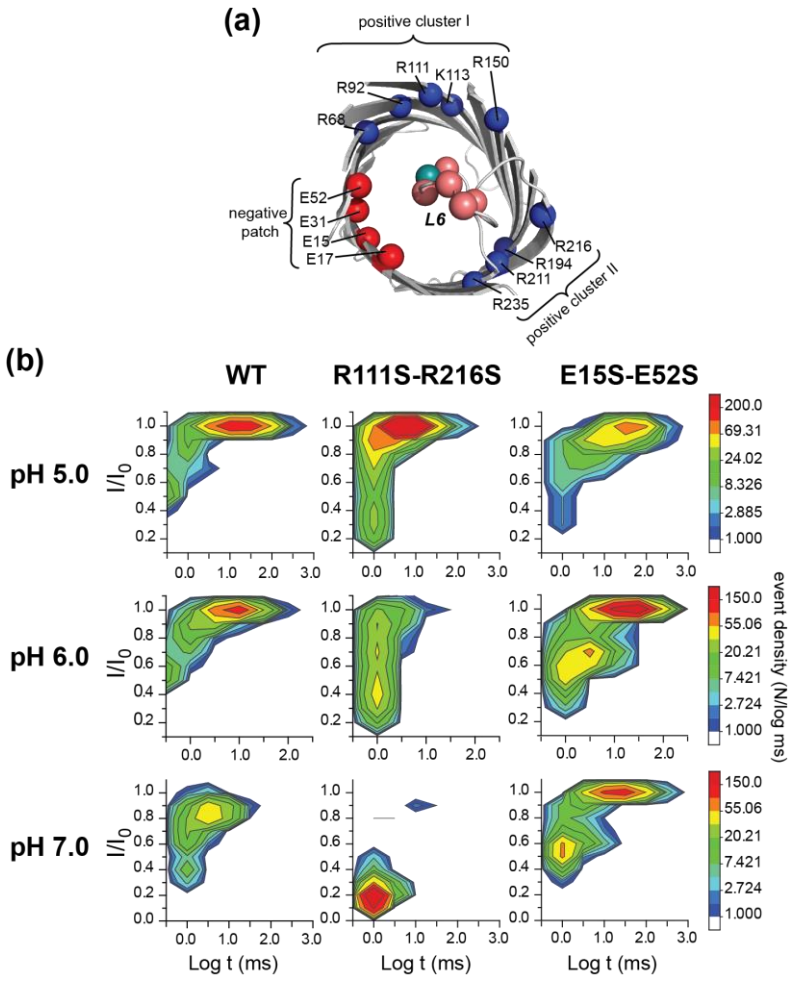

Figure 7. Two-dimensional density contour map of gating events of OmpG variants. (a) OmpG in the closed conformation with barrel and loop 6 residues highlighted. (b) 2-D contour maps of the gating events distribution for the OmpG proteins. The amplitude (I) compared to the fully open state (I_o) is defined as the fraction of current blocked I/I_o on the y axis while the dwell time of the events are in the log scale on the x-axis. The event density is color coded from low (blue) to high (red).

because of the weakened interactions between loop 6 and the diminished positive patch. In contrast, deletion of the negative patch allows loop 6 to easily collapse into the pore and form strong interactions with the positive patch, even at pH 7. This notion is supported by the pH responses of the mutants. As the repulsion decreased with decreasing pH, loop 6 of the mutant R111S-R216S regained the ability to reach the opposite side of the lumen, resulting in longer-amplitude blockages. At pH 5, when the repulsion was the weakest, the mutant R111S-R216S was able to form strong interactions between loop 6 and the remaining residues in the negative

patch, thereby generating 100% blockades. For the mutant E15S-E52S, the protein showed 100% blockages even at pH 7, indicating that loop 6 can cross over the channel entrance in the absence of the repulsion force. Notably, the event distribution of the mutant E15S-E52S was largely insensitive to pH, supporting the notion that the negative patch is the key element for pH sensitivity. In summary, these results strongly suggest that the repulsion between the negative patch and loop 6 control the extent to which loop 6 can bend towards the opposite side of the lumen in order to form stable interactions with the R68-R150 cluster of the positive patch.

DISCUSSION

We have combined computational and experimental approaches to identify key factors that control OmpG pH-dependent gating. During the gross movement of loop 6 in and out the lumen, loop 6 could form multiple interactions with the residues in the lumen or neighboring loops. Identifying these interactions by point mutation is not feasible, as it is both tedious and ineffective. This is because charged residues are clustered on both the lumen and loops. The loss of a specific electrostatic interaction due to a single mutation can easily be compensated for by new interactions with other charged residues nearby.

Our computational analysis allows detailed examination of the ensemble of OmpG loop structures at both pH 5 and pH 7. Our results show that loop 6 is the primary effector of the gating state, which is consistent with conclusions drawn from previous studies.[14,16] In addition, our analysis indicates that loop 6 is the predominant occluder of the OmpG lumen among low-energy closed conformations; further, our model indicates that loop 6–to-barrel interactions play dominant roles in stabilizing these closed conformations (Fig.3a,c) (Supplemental Information, Methods). In particular, we identified a surface patch consisting of highly organized, positively charged residues that provides interactions that favor the closed state at lowered pH (Fig.3b). We have also identified another highly organized surface patch consisting of negatively charged residues E15, E17, E31, and E52, which switches from a charged to a neutral state at lowered pH (Fig.5).

The residues in the negative patch may act as the major pH-sensing element in OmpG gating. This is the first implication that a glutamate cluster is more influential than histidines in pH-sensing.

Consistent with our computational prediction, neutralizing four of the residues in the positive patch not only significantly shifted OmpG to more open states at all pH conditions, but also prevented loop 6 from occluding the pore at pH 7. Thus, our experiments strongly suggest that the role of the positive patch is to stabilize the closed state by attracting loop 6 towards the lumen. Our computational modeling identified the negative patch as the possible pH-sensing element of OmpG. Indeed, electrophysiological experiments revealed that mutants without the negative patch were insensitive to pH change. In addition, the negative patch was found to be responsible for keeping the pore in the open state, presumably by repelling loop 6 out of the lumen.

Based on these results, we propose the following model for the pH-dependent gating of OmpG: the gating of OmpG is primarily derived from the conformational changes of loop 6, which are controlled by a complex electrostatic interaction network formed around loop 6 (Fig. 8). A positive and a negative patch consisting of three highly charged cluster regions are the primary constituents of the electrostatic network that governs OmpG gating. The positive patch attracts loop 6, causing it to bend into the lumen,

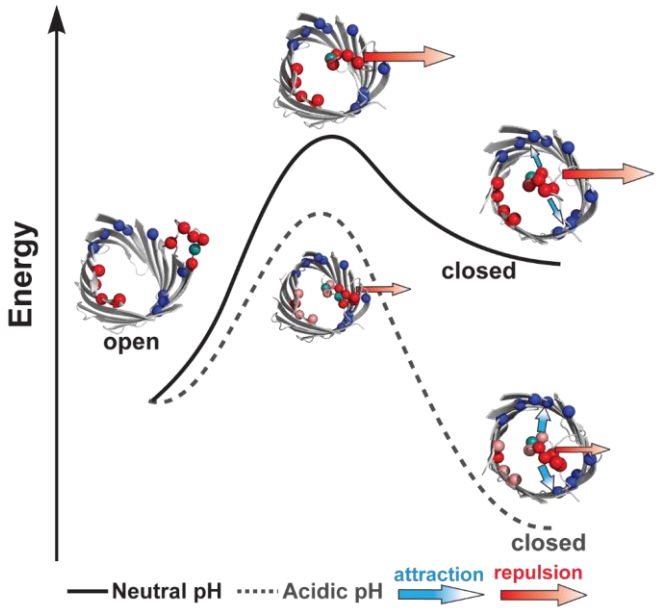

Figure 8. Schematic illustration of the free energy landscape of the OmpG gating process. Repulsion between the negative patch and loop 6 constitutes an energy barrier and destabilizes the closed state. The attraction between positive patch and loop 6 makes the closed state energetically favorable. pH modulates the free energy landscape by adjusting the charge states of the negative patch and residues on loop 6 where they are protonated (pink balls) at acidic pH and deprotonated (red balls) at neutral pH. Cyan balls represent the histidine residues.

while the negative patch, E15-E52, repels loop 6 out of the lumen. The multiple electrostatic interactions between the positive patch and loop 6 energetically stabilize the closed state. Repulsion between the negative patch and loop 6 constitutes an energy barrier for loop 6 to cross the lumen as well as destabilizes the closed state. The attraction and repulsion forces work cooperatively to control the equilibrium of loop 6 gating that is modulated by pH. At neutral pH, the energy barrier is strong so OmpG is trapped mostly in the open state or arrives in a closed state that is energetically less favorable than the open state. As pH is lowered, residues in the negative patch gradually become protonated and uncharged; this lowers the energy barrier as well as the energy of the closed state, thereby allowing loop 6 to invade the lumen and subsequently form highly favorable interactions with the positive surface patch.

In addition to our ensemble analysis of loop structures, the proposed mechanistic model is overall consistent with the computationally predicted crystal structure protonation states for PDBs 2iwv and 2iww. For example, positive patch residues remain protonated at both high and low pH, consistent with our model that this patch is not the pH-sensing element. The negative patch residues E15 and E52 are pH sensors and switch from a deprotonated to a protonated state when pH is decreased; this is consistent with Figure 5. Residues E17 and E31 remain deprotonated and protonated, respectively, and do not contribute to pH sensing in these two structures. While the behavior of residues E17 and E31 in these two X-ray structures alone does not seem to contribute to our proposed mechanism, the conclusion from our ensemble analysis, which does support the role of E17 and E31 as pH sensors (Figures 5, S2), is based on a large population of structures and therefore some variation when examining individual structures is expected.

Notably, our gating model does not exclude the participation of secondary interactions between loop 6 and other groups, such as loop-to-loop attraction and repulsion or histidine repulsion. Although histidine repulsion is not the primary cause of pH-dependent gating, our data clearly suggest that histidines 231 and 261 are involved in promoting the closed state. We surmise

that these two histidines may contribute to the gating in multiple ways. They can destabilize the open state through repulsion to each other, as suggested by Yildiz et. al. Because histidine 231 is located near the positive patch, this residue could also attract loop 6 towards the lumen at acidic pH, and protonated and positively charged H261 may also neutralize the negative charge of loop 6, therefore lowering the energy barrier by reducing the repulsion from the negative patch. Our gating model predicts that a mutant with neutral loop 6 would become insensitive to pH change due to a loss in charged residues that attract and repel the patches, future work of loop 6 mutations will be carried out to further test this model.

In previous studies where loop 6 was fixed,[14] shortened,[37] or pinned to the bilayer,[16] OmpG's spontaneous gating was significantly reduced at pH 7, but not completely eliminated. These studies suggest that mechanisms other than loop 6 motion may also contribute to OmpG's spontaneous gating, such as the motion of other loops or even loop-independent gating such as barrel contraction.[37] In addition to pH-dependent and spontaneous gating, OmpG also exhibited a third class of gating, one that was dependent on the applied voltages in the electrophysiological experiment.[7] It is necessary to distinguish these three types of gating behaviors in electrophysiology, as the voltage-gating may have its own mechanism distinct from the other two. At voltages above ±100 mV, the OmpG pore undergoes a 100% closure which lasts longer than seconds or becomes permanent.[7] In contrast, the dwell times of the spontaneous and pH-gating last between 1 and 50 ms (Fig.3). In our lab, we started to observe the voltage-dependent gating at voltages as low as ±75 mV at pH 7 in 1M KCl (Fig. S9). Loop 6 is unlikely to be associated with the voltage-dependent gating of OmpG, as the deletion of loop 6 and removal of all the loops did not abolish voltage-dependent gating.[37]

Our loop-modeling strategy has aided in unravelling the molecular mechanism of OmpG pH-dependent gating. This is the first report that has identified these significant interactions. Our loop-modeling approach has important advantages over existing computational methods. First,

our measurements show that the average time scale of the gating process is on the order of 10^{-2} s; it is computationally challenging to sample a diverse ensemble of structures on this time scale using molecular dynamics techniques. Our approach samples the conformational space efficiently through the mDiSGro method, which allows greater coverage of the loop conformations involved in the gating process. Second, we can compute the specific protonation state for every sampled conformation. In contrast, molecular dynamics simulations require a fixed protonation state assignment throughout the duration of the conformational sampling simulation. Third, we employ a novel topological approach to assess channel conductance for each of the 10^5 sampled OmpG conformations. This allows a rapid quantification of channel open/closed probability consistent with prior experimental findings[7,15] – a property not previously amenable to computational investigations. Overall, the technical developments employed in our method have enabled us to elucidate the complex molecular mechanisms underpinning pH-dependent OmpG gating. Our approach is generalizable, and can also be useful to study the loop topology of other outer membrane proteins. For example, Opa proteins of *Neisseria gonorrheae* and *Neisseria meningitides* have long loops that are important for bacterial infection and propagation.[38,39] Further studies include refining the energy model for better correlation with the wild type and additional mutant experimental observations. In addition, the large ensemble of loop conformations covering all relevant configurations for gating could be used to develop a detailed theoretical model of kinetic changes among all configurations of the ensemble and to construct detailed transition pathways for gating.

Acknowledgement: This research was supported by the US National Institutes of Health grants R01-GM079804, R01-GM126558 (to JL) and R01-GM115442 (to MC).

References

(1) Delcour, A. H. Outer membrane permeability and antibiotic resistance. *Biochimica et biophysica acta* **2009**, *1794*, 808-816.
(2) Dong, C.; Beis, K.; Nesper, J.; Brunkan-Lamontagne, A. L.; Clarke, B. R.; Whitfield, C.; Naismith, J. H. Wza the translocon for E. coli capsular polysaccharides defines a new class of membrane protein. *Nature* **2006**, *444*, 226-229.
(3) Nikaido, H. Molecular basis of bacterial outer membrane permeability revisited. *Microbiology and molecular biology reviews : MMBR* **2003**, *67*, 593-656.
(4) Pages, J. M.; James, C. E.; Winterhalter, M. The porin and the permeating antibiotic: a selective diffusion barrier in Gram-negative bacteria. *Nature reviews. Microbiology* **2008**, *6*, 893-903.
(5) Bornet, C.; Davin-Regli, A.; Bosi, C.; Pages, J. M.; Bollet, C. Imipenem resistance of enterobacter aerogenes mediated by outer membrane permeability. *Journal of clinical microbiology* **2000**, *38*, 1048-1052.
(6) Lou, H.; Chen, M.; Black, S. S.; Bushell, S. R.; Ceccarelli, M.; Mach, T.; Beis, K.; Low, A. S.; Bamford, V. A.; Booth, I. R.; Bayley, H.; Naismith, J. H. Altered antibiotic transport in OmpC mutants isolated from a series of clinical strains of multi-drug resistant E. coli. *PloS one* **2011**, *6*, e25825.
(7) Conlan, S.; Zhang, Y.; Cheley, S.; Bayley, H. Biochemical and biophysical characterization of OmpG: A monomeric porin. *Biochemistry* **2000**, *39*, 11845-11854.
(8) Subbarao, G. V.; van den Berg, B. Crystal structure of the monomeric porin OmpG. *Journal of molecular biology* **2006**, *360*, 750-759.
(9) Fajardo, D. A.; Cheung, J.; Ito, C.; Sugawara, E.; Nikaido, H.; Misra, R. Biochemistry and regulation of a novel Escherichia coli K-12 porin protein, OmpG, which produces unusually large channels. *Journal of bacteriology* **1998**, *180*, 4452-4459.
(10) Misra, R.; Benson, S. A. A novel mutation, cog, which results in production of a new porin protein (OmpG) of Escherichia coli K-12. *Journal of bacteriology* **1989**, *171*, 4105-4111.
(11) Mari, S. A.; Koster, S.; Bippes, C. A.; Yildiz, O.; Kuhlbrandt, W.; Muller, D. J. pH-induced conformational change of the beta-barrel-forming protein OmpG reconstituted into native E. coli lipids. *Journal of molecular biology* **2010**, *396*, 610-616.
(12) Yildiz, O.; Vinothkumar, K. R.; Goswami, P.; Kuhlbrandt, W. Structure of the monomeric outer-membrane porin OmpG in the open and closed conformation. *The EMBO journal* **2006**, *25*, 3702-3713.
(13) Liang, B.; Tamm, L. K. Structure of outer membrane protein G by solution NMR spectroscopy. *Proceedings of the National Academy of Sciences of the United States of America* **2007**, *104*, 16140-16145.
(14) Chen, M.; Khalid, S.; Sansom, M. S.; Bayley, H. Outer membrane protein G: Engineering a quiet pore for biosensing. *Proceedings of the National Academy of Sciences of the United States of America* **2008**, *105*, 6272-6277.
(15) Zhuang, T.; Chisholm, C.; Chen, M.; Tamm, L. K. NMR-based conformational ensembles explain pH-gated opening and closing of OmpG channel. *Journal of the American Chemical Society* **2013**, *135*, 15101-15113.
(16) Zhuang, T.; Tamm, L. K. Control of the conductance of engineered protein nanopores through concerted loop motions. *Angewandte Chemie* **2014**, *53*, 5897-5902.
(17) Korkmaz-Ozkan, F.; Koster, S.; Kuhlbrandt, W.; Mantele, W.; Yildiz, O. Correlation between the OmpG secondary structure and its pH-dependent alterations monitored by FTIR. *Journal of molecular biology* **2010**, *401*, 56-67.
(18) Conlan, S.; Bayley, H. Folding of a monomeric porin, OmpG, in detergent solution. *Biochemistry* **2003**, *42*, 9453-9465.

(19) Fahie, M.; Chisholm, C.; Chen, M. Resolved single-molecule detection of individual species within a mixture of anti-biotin antibodies using an engineered monomeric nanopore. *ACS nano* **2015**, *9*, 1089-1098.
(20) Reiss, P.; Koert, U. Ion-channels: goals for function-oriented synthesis. *Accounts of chemical research* **2013**, *46*, 2773-2780.
(21) Fahie, M. A.; Yang, B.; Mullis, M.; Holden, M. A.; Chen, M. Selective Detection of Protein Homologues in Serum Using an OmpG Nanopore. *Analytical chemistry* **2015**, *87*, 11143-11149.
(22) Fahie, M. A.; Yang, B.; Pham, B.; Chen, M. Tuning the selectivity and sensitivity of an OmpG nanopore sensor by adjusting ligand tether length. *ACS sensors* **2016**, *1*, 614-622.
(23) Fahie, M. A.; Chen, M. Electrostatic Interactions between OmpG Nanopore and Analyte Protein Surface Can Distinguish between Glycosylated Isoforms. *The journal of physical chemistry. B* **2015**, *119*, 10198-10206.
(24) Tang, K.; Wong, S. W.; Liu, J. S.; Zhang, J.; Liang, J. Conformational sampling and structure prediction of multiple interacting loops in soluble and beta-barrel membrane proteins using multi-loop distance-guided chain-growth Monte Carlo method. *Bioinformatics* **2015**, *31*, 2646-2652.
(25) Tang, K.; Zhang, J.; Liang, J. Fast protein loop sampling and structure prediction using distance-guided sequential chain-growth Monte Carlo method. *PLoS computational biology* **2014**, *10*, e1003539.
(26) Jo, S.; Kim, T.; Iyer, V. G.; Im, W. CHARMM-GUI: a web-based graphical user interface for CHARMM. *Journal of computational chemistry* **2008**, *29*, 1859-1865.
(27) Lomize, M. A.; Lomize, A. L.; Pogozheva, I. D.; Mosberg, H. I. OPM: orientations of proteins in membranes database. *Bioinformatics* **2006**, *22*, 623-625.
(28) Frey, B. J.; Dueck, D. Clustering by passing messages between data points. *Science* **2007**, *315*, 972-976.
(29) Zhang, X. L.; Furtlehner, C.; Sebag, M. Data streaming with affinity propagation. *Machine learning and knowledge discovery in databases* **2008**, 628-643.
(30) Olsson, M. H. M.; Sondergaard, C. R.; Rostkowski, M.; Jensen, J. H. PROPKA3: Consistent Treatment of Internal and Surface Residues in Empirical pK(a) Predictions. *J Chem Theory Comput* **2011**, *7*, 525-537.
(31) Phillips, J. C.; Braun, R.; Wang, W.; Gumbart, J.; Tajkhorshid, E.; Villa, E.; Chipot, C.; Skeel, R. D.; Kale, L.; Schulten, K. Scalable molecular dynamics with NAMD. *Journal of computational chemistry* **2005**, *26*, 1781-1802.
(32) Huang, J.; MacKerell, A. D. CHARMM36 all-atom additive protein force field: Validation based on comparison to NMR data. *Journal of computational chemistry* **2013**, *34*, 2135-2145.
(33) Dundas, J.; Ouyang, Z.; Tseng, J.; Binkowski, A.; Turpaz, Y.; Liang, J. CASTp: computed atlas of surface topography of proteins with structural and topographical mapping of functionally annotated residues. *Nucleic Acids Res* **2006**, *34*, W116-W118.
(34) Bondi, A. Van Der Waals Volumes + Radii. *J Phys Chem-Us* **1964**, *68*, 441-451.
(35) Benjamini, Y.; Yekutieli, D. False discovery rate-adjusted multiple confidence intervals for selected parameters. *J Am Stat Assoc* **2005**, *100*, 71-81.
(36) Fitch, C. A.; Platzer, G.; Okon, M.; Garcia-Moreno, B. E.; McIntosh, L. P. Arginine: Its pKa value revisited. *Protein science : a publication of the Protein Society* **2015**, *24*, 752-761.
(37) Grosse, W.; Psakis, G.; Mertins, B.; Reiss, P.; Windisch, D.; Brademann, F.; Burck, J.; Ulrich, A.; Koert, U.; Essen, L. O. Structure-based engineering of a minimal porin reveals loop-independent channel closure. *Biochemistry* **2014**, *53*, 4826-4838.
(38) Fox, D. A.; Larsson, P.; Lo, R. H.; Kroncke, B. M.; Kasson, P. M.; Columbus, L. Structure of the Neisserial outer membrane protein Opa(6)(0): loop flexibility essential to receptor recognition and bacterial engulfment. *Journal of the American Chemical Society* **2014**, *136*, 9938-9946.

(39) Hauck, C. R.; Meyer, T. F. 'Small' talk: Opa proteins as mediators of Neisseria-host-cell communication. *Current opinion in microbiology* **2003**, *6*, 43-49.
(40) Tang, K.; Zhang, J.; Liang, J. Distance-Guided Forward and Backward Chain-Growth Monte Carlo Method for Conformational Sampling and Structural Prediction of Antibody CDR-H3 Loops. *Journal of chemical theory and computation* **2016**, *13*, 380-388